EMPIR
The EMPIR initiative is co-funded by the European Union's Horizon 2020 research and innovation programme and the EMPIR Participating States

Low-power measurement using diode type power sensors in the presence of higher harmonics

Document Type: Best ptactice guide

Authors: K. Dražil[1], A. K. Dogan[2], M. Celep[2], J. Grajciar[1], T. Pavlíček[1], M. Hudlička[1], A. R. Sallam[3], B. Pinter[4], M. Rodríguez[5]

Activity Partners: CMI[1], TUBITAK/UME[2], NIS[3], SIQ[4], INTA[5]

February 2019

CONTENTS

1. Introduction

At RF and microwave frequencies, power has been adopted as the primary amplitude measurement quantity for the signal. The traceability of microwave power to SI units is provided through a microcalorimeter setup typically around 0 dBm nominal power [1] with thermistor sensors used as transfer standards. Thermistor sensors are suitable for the most accurate power measurements in metrological laboratories but they are not very suitable for most practical applications [2], [3]. One of the main limitations of thermistors includes their low dynamic range (max. 30 dB). For most applications, diode-type power sensors (DTPS) with significantly higher dynamic range (50 dB to 90 dB) are widely used allowing power levels in the range -70 dBm to +20 dBm to be measured. There are currently various types of DTPSs with different internal architecture which are optimized for various applications. This guide shows a method of evaluation of measurement errors caused by the presence of higher order harmonics when measured with DTPS.

2. Diode type power detector

Diode sensors use high-frequency semiconductor diodes to detect the RF voltage developed across a terminating load resistor. A diode is a two-terminal electronic component that conducts primarily in one direction; it has a low resistance to the flow of current in one direction, and high resistance in the other. A semiconductor diode, the most common type today, is a crystalline piece of semiconductor material with a p-n junction connected to two electrical terminals. At levels below –20 dBm (22 mV rms input voltage in a 50 Ω system), typical RF diode detectors produce a DC voltage output that is nearly proportional to the square of the applied RF voltage. This is referred to as the square-law or true-rms region. Above 0 dBm, a linear detection (i.e. peak detection) region exists where the output voltage is almost proportional to the input voltage. The transition region of the detectors ranges from approximately –20 dBm to 0 dBm of input power. The voltage-current characteristic of a diode is shown in Fig. *1*.

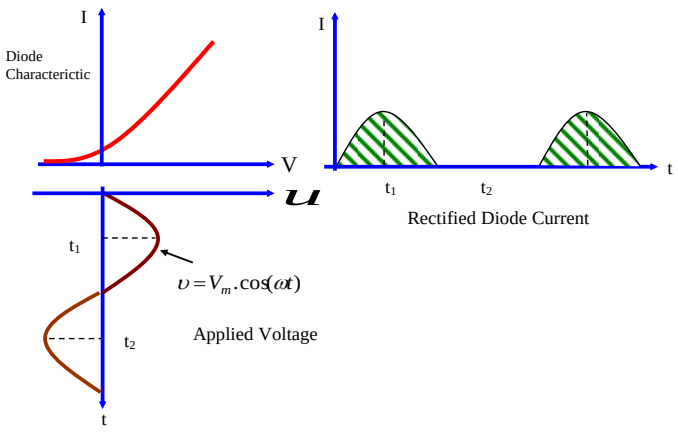

Fig. 1. Voltage-current characteristic of a diode.

The diode equation gives an expression for the current through a diode as a function of voltage. The *ideal diode law* is expressed as:

$$I = I_0\left(e^{\frac{\upsilon}{V_0}} - 1\right) \tag{1}$$

where $\upsilon = V_m \cos \omega t$ is the applied voltage across the diode and V_0 is thermal voltage.

Eq. 1 is rewritten according to the exponential characteristic of the diode as following:

$$I = I_0\left(e^{\frac{\upsilon}{V_0}} \text{-1} \right) = I_0\left[\frac{V_m}{V_0} cos\,\omega t + \frac{1}{2}\left(\frac{V_m}{V_0}\right)^2 cos^2\,\omega t + \frac{1}{8}\left(\frac{V_m}{V_0}\right)^3 cos^3\,\omega t + ... \right] \quad (2)$$

In this equation:

- I: Diode current
- I_0: Leakage current
- $V_0 = \frac{k.T}{e} = constant$: Thermal voltage
- k: Boltzmann constant
- T: Temperature (K)
- e: Electron charge

The expansion of the exponential function of Eq. 2 is taken into account as below;

$$e^{\frac{\upsilon}{V_0}} = e^{\frac{V_m}{V_0} cos\,\omega t} = 1 + \frac{V_m}{V_0} cos\,\omega t + \frac{\left(\frac{V_m}{V_0} cos\,\omega t\right)^2}{2!} + ... \quad (3)$$

And also taking into account the use of the trigonometric property given below in Eq. 4;

$$cos^2\,\omega t = \frac{1}{2}\left(1 + cos\left(2\omega t\right)\right) \quad (4)$$

The current passing through the diode is calculated as follows;

$$I = 0.25 I_0\left(\frac{V_m}{V_0}\right)^2 + I_0\left(\frac{V_m}{V_0}\right) cos\,\omega t + 0.25 I_0\left(\frac{V_m}{V_0}\right)^2 cos\,2\omega t + ... \quad (5)$$

Eq. 5 has two components; one of them is DC and the others are AC component. Therefore,

$$I = I_{DC} + I_{AC} \quad (6)$$

DC current is obtained as in Eq. 7;

$$I_{DC} = 0.25 I_0\left(\frac{V_m}{V_0}\right)^2 \quad (7)$$

There are constants in parenthesis

$$I_{DC} = \left(\frac{0.25 I_0}{{V_0}^2}\right) {V_m}^2$$

The DC component of current is proportional with the square of the applied voltage magnitude;

$$I_{DC}\ \alpha\ {V_m}^2 \quad (8)$$

Since microwave power, P_m, is also proportional to the square of the voltage, it is also proportional to the DC current.

$$P_m \alpha V_m^2 \tag{9}$$

$$\left.\begin{array}{l} P_m \alpha V_m^2 \\ I_{DC} \alpha V_m^2 \end{array}\right\} \Rightarrow P_m \alpha I_{DC} \tag{10}$$

Since microwave power is proportional with the DC current passing through diode. Eq. 7 is called “the square law”. So the square-law region of diode sensors is the range of the power proportional to the square of the voltage.

When operating in the square-law region, detectors tend to measure true rms power. If a non-sinusoidal signal is to be measured, higher harmonics are weighted according to their power and the error due to harmonics is negligible. However, with increasing power level, the diode detector changes from rms weighting to peak weighting of the input voltage and the error due to harmonics can significantly increase with dependence on the mutual phase between the fundamental and higher harmonic signal. Graphic presentation of typical behaviour for the R&S DTPS with respect to second and third harmonics can be found in [2], see Fig. *2* for a full-wave and half-wave rectification. Measurement errors can be either positive or negative depending on the phase of the harmonics. The uncertainties for diode type sensors are briefly mentioned also in application note [4].

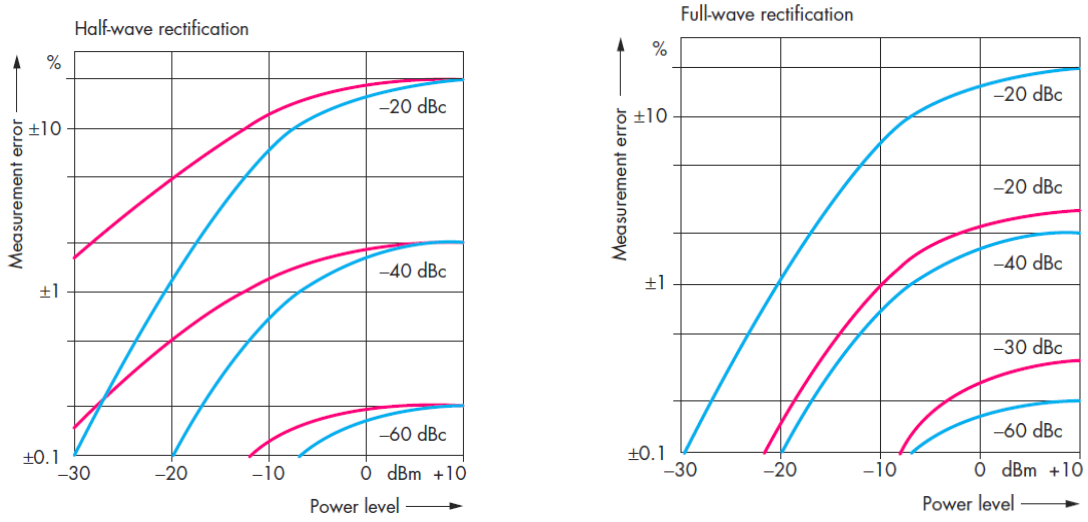

Fig. 2. Typical measurement errors due to higher harmonics for R&S diode sensors [2].

The error cannot be reduced by a low-impedance load of the rectifier. It can be improved with full-wave rectifiers by taking the average value from the positive and negative voltage peaks, thus eliminating the effect of even-numbered harmonics, in particular, that of 2nd orders. As shown in Fig. *2*, considerable measurement errors may occur with half-wave rectification even within the square-law region. The most natural solution how to reduce the effect of higher harmonic components to the measured power error is to use a bank of filters for different frequency bands, which remove the unwanted spectral components. The insertion of a filter, however, introduces new potential mismatch error source, which must be eliminated mathematically.

Historically, older types of diode power sensors were designed only for operation in the square-law regime with dynamic range approx. 50 dB (e.g. the HP 8484A and Agilent 8481D sensors). With the progress of electronics, it was feasible to construct power sensors featuring detector shaping compensation (for CW) to extend the dynamic range above the square-law region up to 90 dB (e.g. the R&S NRV-Zx, Agilent ECP-26A, Agilent E441x or Anritsu MA244xD sensors). An example of the internal architecture of the Agilent E4412/13A sensor is shown in Fig. *3*. There are also latter multipath diode sensors that integrate multiple

diode detectors and attenuating power splitters into a single unit. These sensors operate usually with two or three pairs of detectors and select the output of whichever pair is operating in its square-law region. Examples of such architecture include the R&S NRP-Zxx sensors, Keysight U2040 X series or Anritsu MA2480D series sensors, respectively.

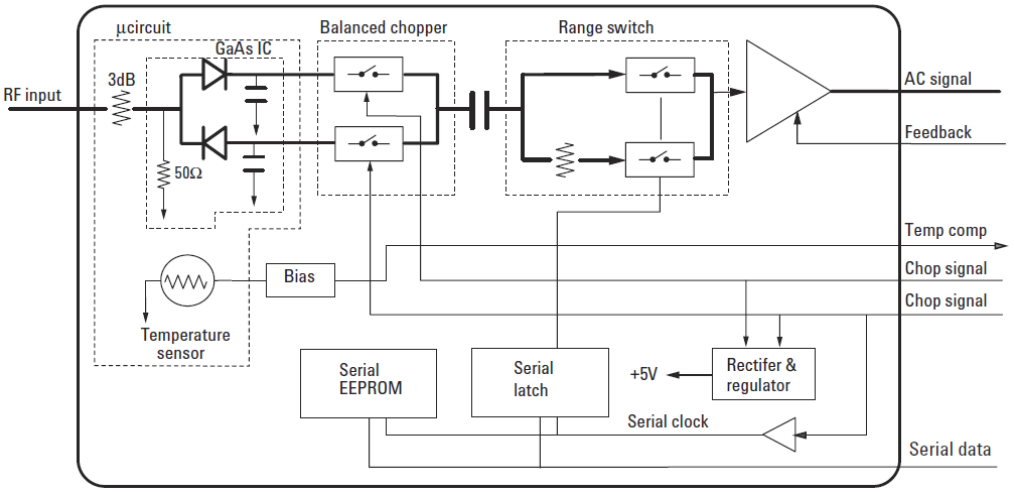

Fig. 3. Internal architecture of the Agilent E4412/13A power sensor [3].

Making power measurements in the transition and linear regions of the diode response is less accurate when the signal input is modulated with wide bandwidth signals or multiple tone signals. To make these measurements, the instrument must have the dynamic measurement power range and the frequency response to be quantifiable, repeatable and correctable. For the diode sensors, extensive EEPROM correction tables are used for the frequency, signal levels and temperatures at which the power measurements will be made. In many cases, these corrections are not adequate for very wideband devices such as Ultra Wideband USB or some of the other digital modulation formats. Most sensors have an instantaneous bandwidth that they can respond to which typically range from 10 MHz to 30 MHz. With modulation formats wider than this and higher in power than the square law region, pulsed power or sensor instantaneous bandwidth can have varying amounts of error.

Although some types of DTPS are, under certain conditions, highly susceptible to errors due to harmonics, data supplied by manufacturers are often very limited. Detailed information is only available for R&S power sensors where the software [5] is available, which allows evaluating the measurement uncertainty contributions due to the 2nd and 3rd harmonics. Another source of error in diode sensors is the temperature. The ambient temperature affects the performance of a diode detector in three ways [6]. Firstly, it causes a variation in the RF impedance of the diode. Secondly, the optimum DC load resistance varies with temperature in order to preserve a square law response over a range of temperatures and a temperature-dependent load is desirable. Thirdly, the voltage responsivity will be temperature-dependent and this effect must be compensated for. Changes of output with temperature ranging from -0.15 per cent to +2.5 per cent per degree C. In modern power meters, these changes are compensated using a look-up table stored in the sensor's EEPROM memory [2].

It is very impractical to characterize a diode sensor for all possible input power levels and levels of the higher harmonic signal. In this Guide, a method is described which allows characterizing a sensor by means of only several measurements and semi-analytical relations. A detailed description of diode power sensor characterization is given in [7]. In this Guide, a more practitioner-oriented description of the whole characterization process is provided.

3. Modelling of errors due to harmonics in diode detectors

Modern diode power sensors make use of low-barrier Schottky (LBS) [8], planar doped barrier (PDB) diodes [9] or modified barrier integrated diodes (MBID) [10]. The ideal I-V characteristic of a detecting diode is given in Eq. (1). It can be re-written as

$$i_d = I_S\left(e^{\alpha v_d} - 1\right), \tag{11}$$

where $\alpha = q/nkT$ and I_S is the saturation current, q is the electron charge, k is the Boltzmann constant, T is the absolute temperature and n is the ideality factor. For a typical detector, $I_S \approx$ 10 μA, $n \approx 1.1$ [3]. Eq. (11) is often written as the power series

$$i_d = I_S\left(\alpha v_d + \frac{(\alpha v_d)^2}{2!} + \frac{(\alpha v_d)^3}{3!} + \ldots\right). \tag{12}$$

For the purposes of this guide, the detectors are modelled without frequency-dependent elements. A simplified circuit used for modelling is shown in Fig. *4*.

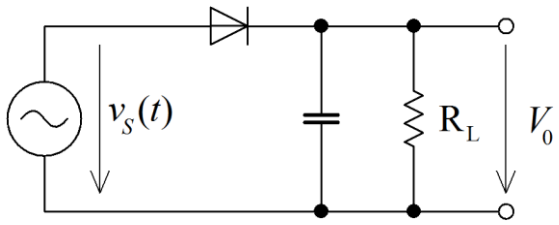

Fig. 4. Simplified equivalent circuit of a single-diode detector.

The signal with higher harmonics used for investigation is defined as

$$v_S(t) = V_m\left(\sin(\omega t) + r\sin(m\omega t - \varphi_m)\right), \tag{13}$$

where V_m is the amplitude of the signal at the fundamental frequency, m is the order of the higher harmonic component, r is the amplitude ratio between the higher and fundamental harmonic components and φ_m is the phase shift of the m-th harmonic component.

The capacitor in Fig. *4* is regarded as large enough to keep only the DC voltage. The average current through the diode can be solved by integrating over one RF cycle

$$\frac{1}{T}\int_0^T i_d(t)\,dt = \frac{V_0}{R_L}, \tag{14}$$

where V_0 is the DC voltage at the output of the detector. For the detector with an ideal diode in Fig. *4*

$$i_d(t) = I_S\left(e^{\alpha(v_S(t) - V_0)} - 1\right). \tag{15}$$

By solving the Eq. 13, Eq.14 and Eq.15 numerically, the values for the maximum measurement error of single-diode detectors can be calculated. First, values of detector output voltage V_0 are found iteratively for CW signal and various input voltage levels (presented in dBm at 50 Ω load). Subsequently, the values of total input power are found for the same levels of output voltage V_0, defined harmonic-to-fundamental ratios and various phase shifts. The results obtained are shown in Fig. 5 and Fig. 6.

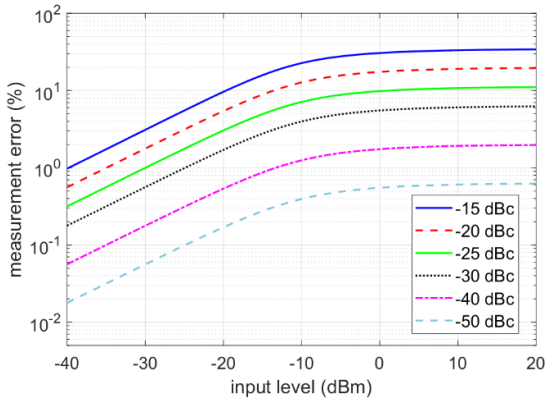

Fig. 5. Modelled worst case errors due to 2. harm., half-wave detector.

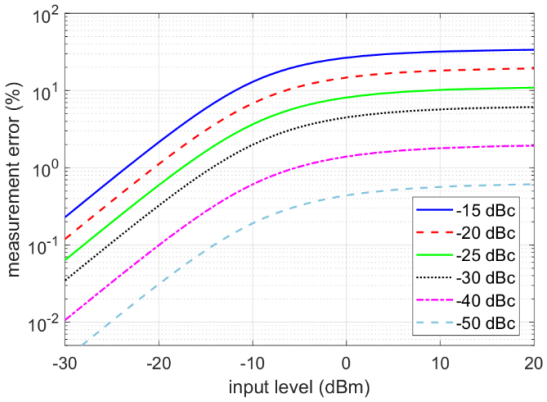

Fig. 6. Modelled worst case errors due to 3. harm., both detector types.

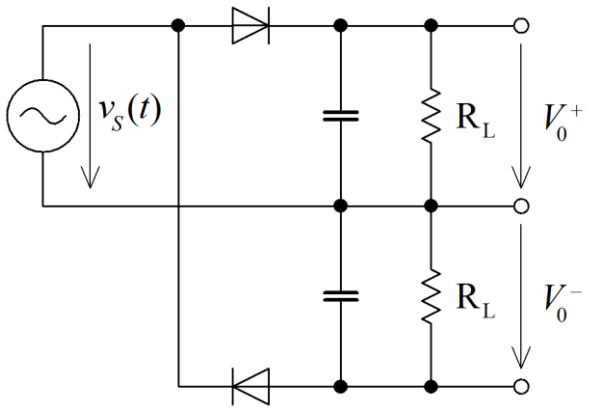

Fig. 7. Simplified equivalent circuit of the full-wave (balanced) detector.

A simplified schematic diagram of a balanced detector with full-wave rectification can be seen in Fig. *7*. The detected voltage is now the sum of V_0^+ and V_0^-. As shown in [11], such a detector represents a peak-to-peak rather than just a peak detector for large signals and its sensitivity to the second (and any other even) harmonic is reduced when compared to the single diode detector. Similarly, we modelled the results for the balanced detector as seen in Fig. *8*.

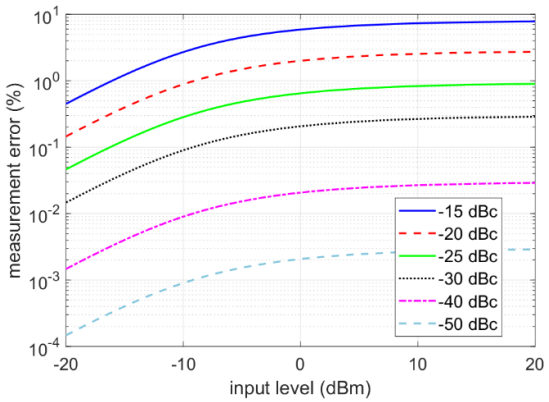

Fig. 8. Modelled worst-case errors due to 2. harm., full-wave detector.

Results obtained for the detectors with diodes modelled as the exponential device according to (Eq. 15) can be concluded as follows. Resulting measurement errors due to harmonics seem to be independent on the detector loading resistance R_L. For small R_L,

unrealistic current peaks have been calculated as a consequence of neglecting the resistance in series with the ideal diode model. The shape of the resulting curves in logarithmic scale reveals asymptotic characteristics where the horizontal asymptotes represent the error limits ($\delta \approx 2r$) corresponding to the expected peak detecting behaviour of the detectors. Only the horizontal shift of the curves was observed when α was changed. Resultant measurement errors due to harmonics are in very good agreement with those presented in [2].

Fig. 6 shows the model including resistors R_S representing the equivalent Thévenin resistance of the source and ohmic resistance of the diodes. The numerical results obtained by solving the circuit in Fig. *9* can be seen in Fig. 10 and Fig. 11 where the effect of the detector load is visible. The effect of the reverse diode current for PDB diodes given in [3] was also modelled.

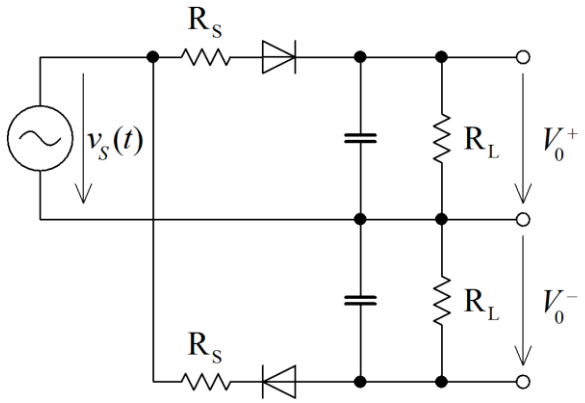

Fig. 9. Equivalent circuit of the balanced detector.

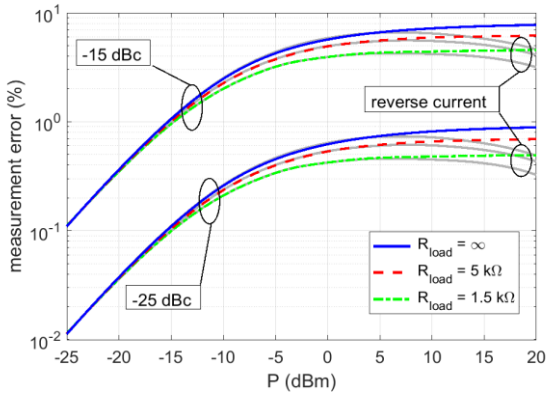

Fig. 10. Modelled worst-case errors due to 2. harm., full-wave detector.

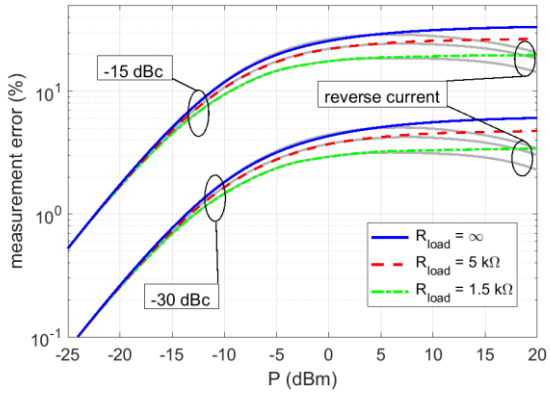

Fig. 11. Modelled worst-case errors due to 3. harm., both detector types.

On the basis of the results, it can be concluded that detectors deviate from the peak detecting behaviour with decreasing loading resistance. This effect can be enforced when the voltage across the diode approaches the breakdown region.

Real diode circuits used in power sensors generally use the architecture from Fig. *4* or Fig. *9*, however, there may be other reactive compensation elements and the diode itself can be described using a much more complicated model [12]. The true diode architecture used in commercial power sensors is not publicly available. SPICE models of a general Schottky diode and several detector circuits are available in commercial circuit simulators (see e.g. [13]). An example of a simulation of the HSMS-286x Series Surface Mount Microwave

Schottky Detector Diode from Agilent Technologies [14] in the Agilent ADS simulator is shown in Fig. *12*. In order to obtain a realistic diode sensor equivalent circuit, the real diode model could be obtained by measurement of the I-V characteristics in forward and reverse direction, changing temperature, changing bias voltage, changing input power (small + large signal analysis) and other parameters and then optimizing the SPICE model values in order to get good agreement with the measurements. Such a procedure, however, is not realistic without specialized measurement equipment.

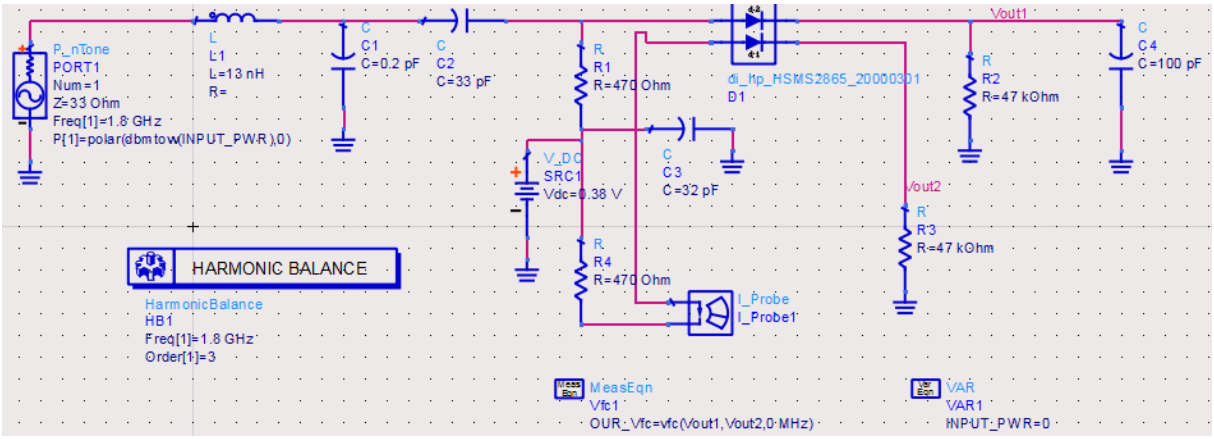

Fig. 12. Modeling a commercial HSMS-2865 diode pair circuit as a full-wave detector.

4. Modelling using the approximating formula

The aim of was to find a general approximating formula which can help the users to predict the behaviour of sensors with respect to harmonics on the basis of only several measurements, instead of characterizing the detector for all possible power levels of the fundamental and higher harmonics. Based on the characteristics of the curves, the formula was proposed in the form

$$\delta\ (\%) = kr^{er}\left[\left(\frac{P_m}{P}\right)^{ep_1 ep_2} + 1\right]^{\frac{1}{ep_2}}, \tag{16}$$

where δ is the maximum measurement error in (%), P is the power level in mW, r is the higher harmonic suppression, P_m and k are constants optimized for the best fit to the measured or modelled values, ep_2 does influence the bending of the curves and is usually optimized only for the best fit to the modelled values (see Table 1) and er, ep_1 are fixed constants chosen depending on the harmonic order and detector type (see Table 1). When the sensor is to be characterized on the basis of measurement, P_m and k are optimized separately for the second and third harmonic.

Parameter	2. harm.		3. harm	sensors
	full-wave detector	half-wave detector		
er	2	1	1	
ep_1	1	0.5	1	
ep_2	0.77	1.86	0.85	NRV-Zx
	0.99		1.15	ECP-E26A E4413A

Table 1. Constants for the approximating formula.

The results obtained by detector modelling and by Eq. (16) are compared in graphs shown in Fig. 13 to Fig. 17. Results for the detectors with large loading resistance (i.e. with

peak detecting behaviour) can be seen in Fig. 13 to Fig. 15. In Fig. 16 and Fig. 17, results for the hypothetical model of the sensor ECP-E26A are compared. This sensor includes 3 dB attenuator at the input, further elements of the model R_S = 50 Ω, R_L = 1.4 kΩ and the reverse current of the diodes equal to 4 mA @ 4 V (see [3]) were supposed. It can be seen that the formula gives acceptable results even for the sensors which do not show the peak detecting behaviour with the potential deviations at levels above 10 dBm taken into account where appropriate.

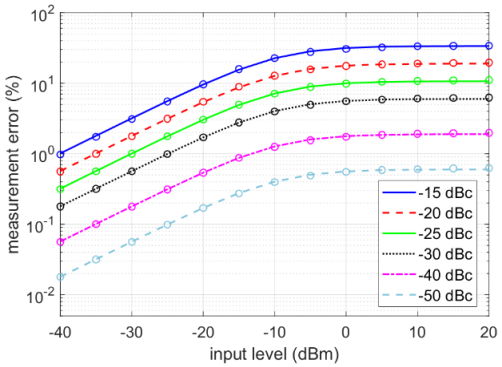

Fig. 13. Worst case errors due to 2. harm., half-wave detector, lines = fit by (6), circles = detector model, large R_L.

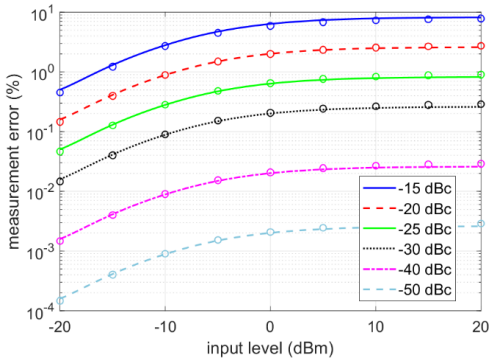

Fig. 14. Worst case errors due to 2. harm., full-wave detector, lines = fit by (6), circles = detector model, large R_L.

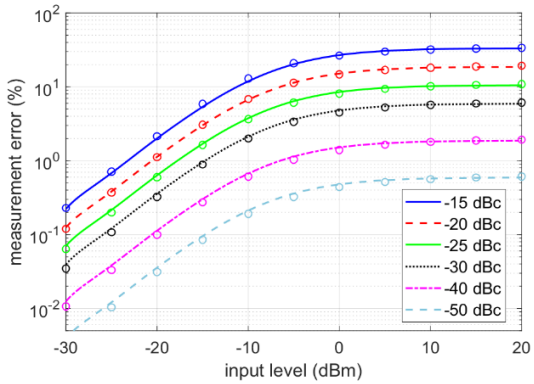

Fig. 15. Worst case errors due to 3. harm., lines = fit by (6), circles = detector modelling, large R_L.

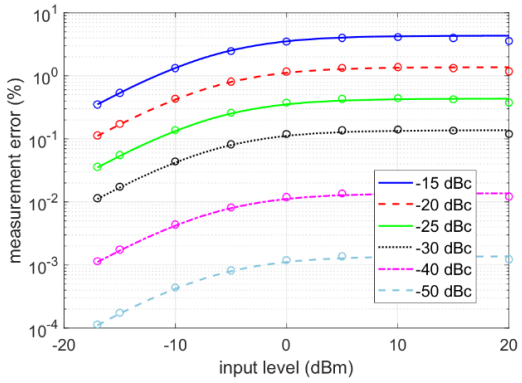

Fig. 16. Worst case errors due to 2. harm., full-wave detector, lines = fit by (6), circles = detector model, RL=1.4 kΩ, reverse diode current taken into account.

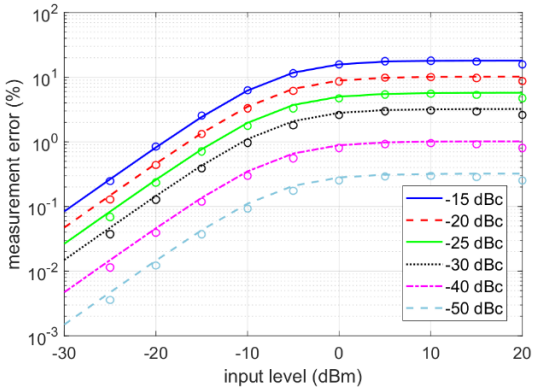

Fig. 17. Worst case errors due to 3. harm., lines = fit by (6), circles = detector model, R_L=1.4 kΩ, reverse diode current taken into account.

5. Measurement method

The measurement method is based on the fact that the indication of the power meter with DTPS operating above the square-law region is dependent on the phase shift between the fundamental and higher harmonic components. The measurement setup consists of two RF generators (the fundamental and the higher harmonic components), and a coupling device which creates a composite signal. Sufficient isolation of both generators is provided and a set of filters can optionally be used to suppress the unwanted higher order harmonics of the fundamental frequency. The use of phase-locked synthesizers is necessary as the phase shift between the fundamental and higher harmonic component must be adjusted to obtain a maximum/minimum reading of the power meter. The phase shift can be changed between 0° and 360° either directly in the generator (certain types of RF generators have this functionality) or by slightly detuning the frequency of the second generator (approx. 1 Hz to 10 Hz). The detuning creates a slowly varying change of the power meter reading so that the user can easily monitor the minimum/maximum power reading. Another possibility is to add a suitable variable phase shifter to the input of the reference signal 10 MHz of one of the used synthesizers. The alternative measurement configurations are shown in Fig. *18* and Fig. *19*. The two-resistor power splitter is used as it yields better isolation between the generators in comparison with the 3-resistor power divider. The alternative approach with the directional coupler is suitable namely for measurements at higher power levels. If the influence of both second and third harmonics needs to be evaluated, a modified setup with three signal generators can be used, see Fig. *20*. For very low power levels of the fundamental frequency, the dynamic range of the spectrum analyzer may not be sufficient to measure the level of the 2nd or 3rd harmonics.

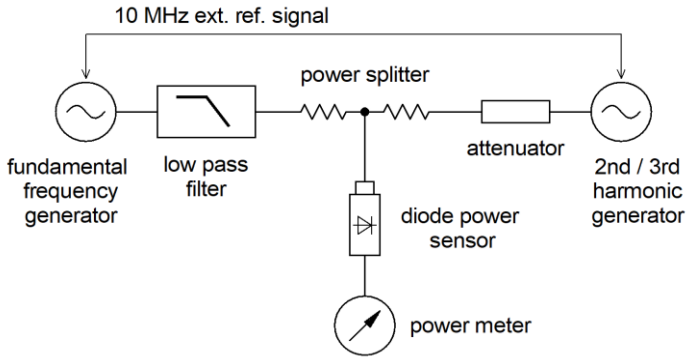

Fig. 18. Setup for characterization of DTPS with a power splitter.

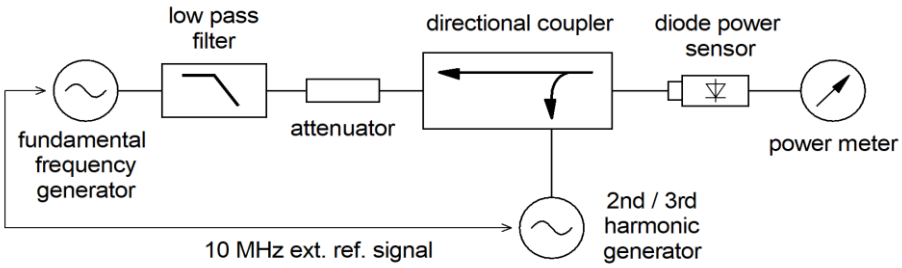

Fig. 19. Setup for characterization of DTPS with a directional coupler.

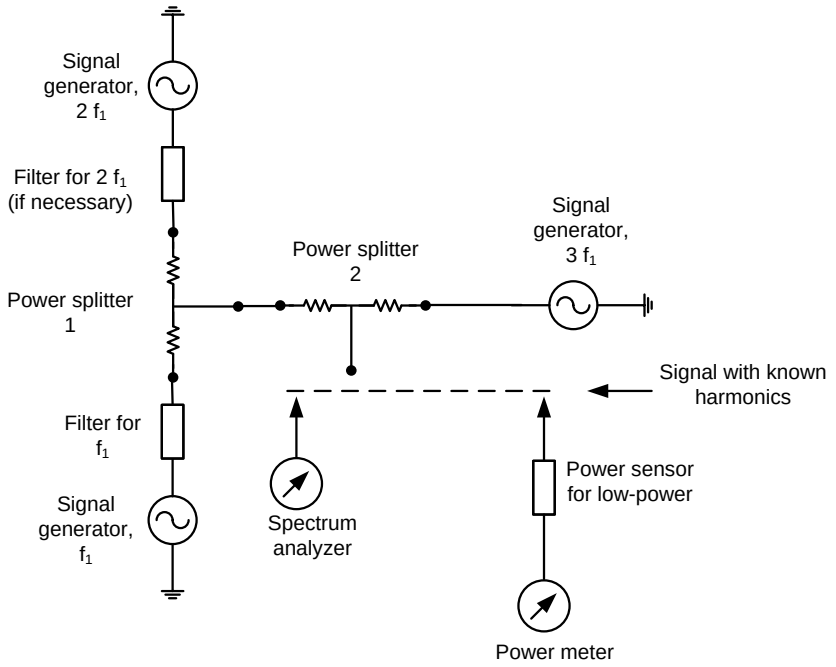

Fig. 20. Setup for characterization of DTPS with a power splitter and sources of signal with known second and third harmonics.

In order to determine the worst case power indication error, it is necessary to find the maximum (P_{max}) and minimum (P_{min}) indicated power when both the fundamental and higher order harmonic components are present and also when only the fundamental component is present (P_c). Note that the positive and negative errors are not symmetrical and the larger of them (in magnitude) is to be selected as the result [11]. The positive and negative errors δ_+, δ_-, respectively, can be calculated by

$$\delta_+(\%) = \left(\frac{P_{\max}}{P_c\left(1+r^2\right)} - 1 \right) \cdot 100 \tag{17}$$

and

$$\delta_-(\%) = \left(\frac{P_{\min}}{P_c\left(1+r^2\right)} - 1 \right) \cdot 100\,, \tag{18}$$

where r is the amplitude ratio between the higher and fundamental harmonic components.

6. Measurement examples

The characterization of the influence of higher harmonic components on the power error was performed for various commercial DTPS from different vendors. Properties of sensors with both half-wave and full-wave detectors, respectively, were evaluated. Fig. 21 and Fig. 22 show the results for the R&S NRV-Z1 sensor (half-wave detector). This sensor shows the peak detecting behaviour.

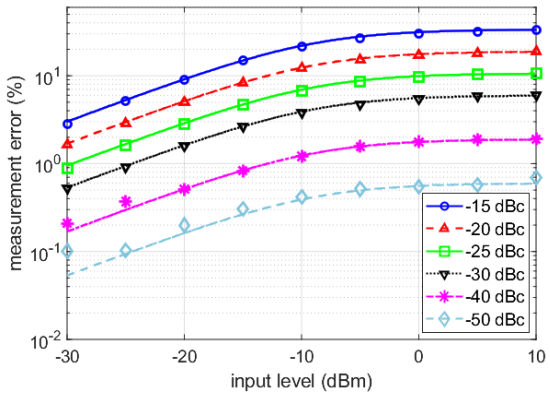

Fig. 21. Modelled and measured worst-case errors due to 2. harm. (R&S NRV-Z1 sensor), lines = fit by (6), symbols = measured (f = 2.5 GHz).

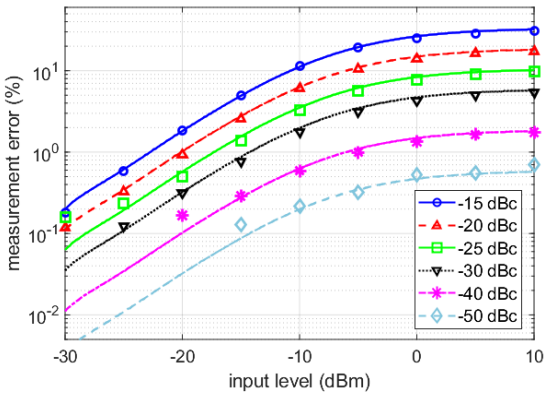

Fig. 22. Modelled and measured worst-case errors due to 3. harm.(R&S NRV-Z1 sensor), lines = fit by (6), symbols = measured (f = 2.5 GHz).

Fig. 23 and Fig. 24 show the results for the R&S NRV-Z4 sensor (full-wave detector). This sensor also shows the peak detecting behaviour.

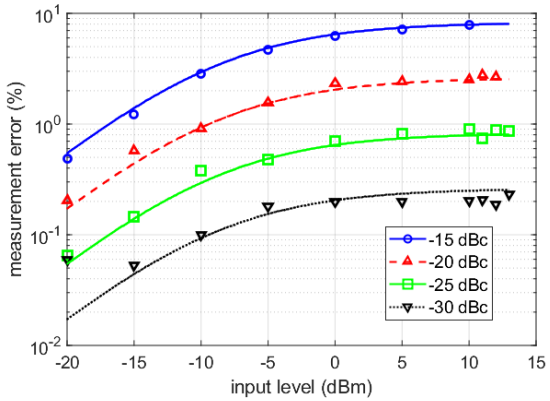

Fig. 23. Modelled and measured worst-case errors due to 2. harm. (R&S NRV-Z4 sensor), lines = fit by (6), symbols = measured (f = 2.5 GHz).

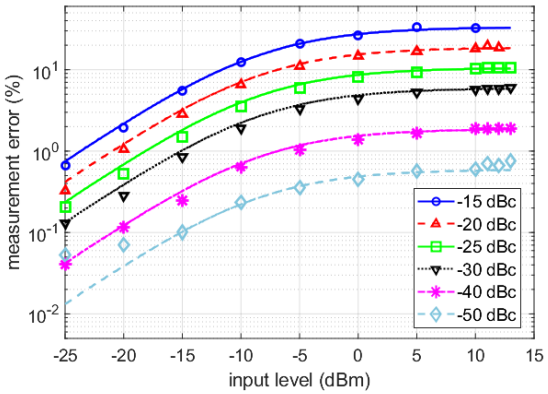

Fig. 24. Modelled and measured worst-case errors due to 2. harm. (R&S NRV-Z4 sensor), lines = fit by (6), symbols = measured (f = 2.5 GHz).

Fig. 25 and Fig. 26 show the results for the HP 8484A sensor (half-wave detector). The characteristics of the sensor cannot be completely fitted as the measurement above the square-law region is not supported by the manufacturer.

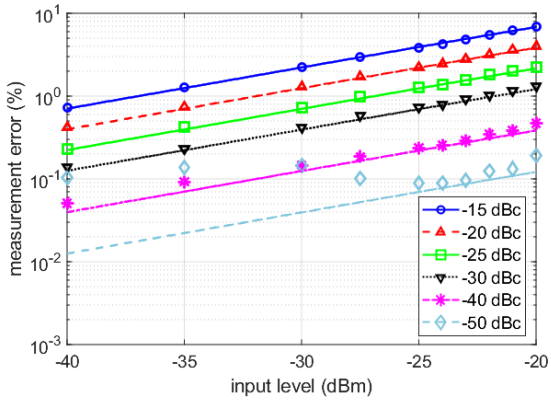

Fig. 25. Modelled and measured worst-case errors due to 2. harm. (HP 8484A sensor), lines = fit by (6), symbols = measured (f = 2.5 GHz).

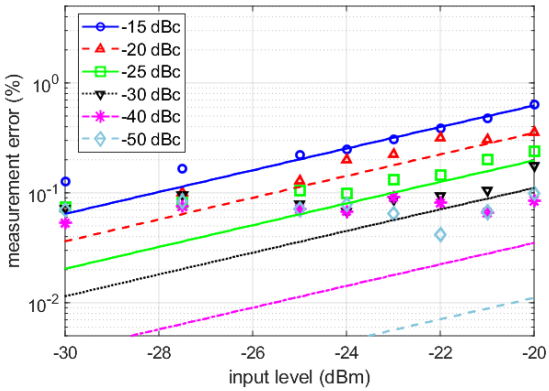

Fig. 26. Modelled and measured worst-case errors due to 3. harm. (HP 8484A sensor), lines = fit by (6), symbols = measured (f = 2.5 GHz).

Fig. 27 and Fig. 28 show the results for the sensor HP ECP-E26A (full-wave detector). This sensor does not show peak detecting behaviour.

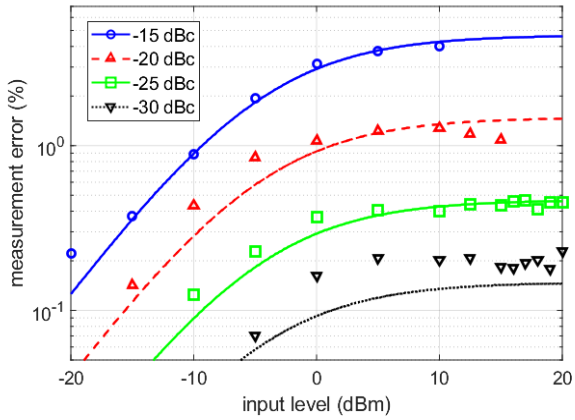

Fig. 27. Modelled and measured worst-case errors due to 2. harm. (HP ECP-E26A sensor), lines = fit by (6), symbols = measured (f = 2.5 GHz).

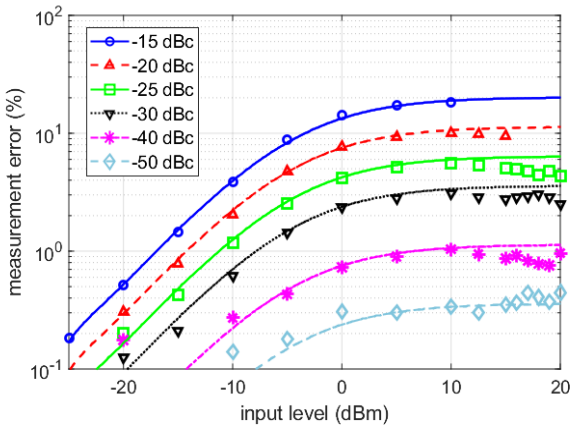

Fig. 28. Modelled and measured worst-case errors due to 3. harm. (HP ECP-E26A sensor), lines = fit by (6), symbols = measured (f = 2.5 GHz).

Fig. 29 and Fig. 30 show the results for the sensor Agilent E4413A (full-wave detector). This sensor does not show peak detecting behaviour.

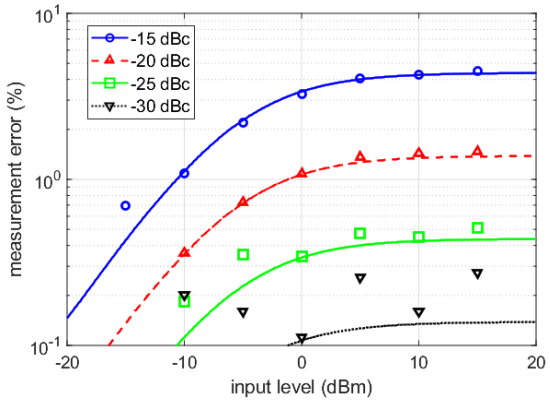

Fig. 29. Modelled and measured worst-case errors due to 2. harm. (Agilent E4413A sensor), lines = fit by (6), symbols = measured (f = 5 GHz).

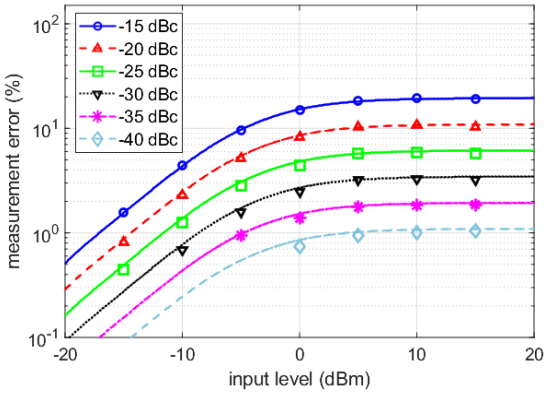

Fig. 30. Modelled and measured worst-case errors due to 3. harm. (Agilent E4413A sensor), lines = fit by (6), symbols = measured (f = 5 GHz).

7. Potential sources of errors in the evaluation of the sensitivity to harmonics

For practical purposes, the errors caused by the higher harmonics content should only be considered if their size is greater or comparable to other error sources.

When verifying the proposed method, measurements in the region of relatively small expected errors were also performed. Errors in the order of tenths of per cent caused by higher harmonics are considered as negligible in practice. As given in Section 5, the errors caused by higher harmonics are evaluated from the changes of the power meter indication, where it is ideally assumed that the changes are only caused by the phase shift change or by switching off the source of the higher harmonic. In the measurements, changes due to noise, zero drift, power meter resolution and generator output level instability are also evaluated including the influence caused by higher harmonics. These influences tend to be more

important for signals with increasing harmonic suppression. In this way, e.g. differences shown in Fig. 26 can be explained.

The measurement setup in Fig. *18* and Fig. *19* is suitable for frequencies, at which the higher harmonic suppression can be determined using the measured sensor which is capable of working at 2 or 3 times of the fundamental frequency. If this condition is not fulfilled, another equipment for measurement of the level of higher harmonics must be used. It is necessary to keep in mind that the diode sensor connectors are not designed to support the higher harmonic frequencies, where the connector will become over-moded. As a consequence, the harmonic response may not be repeatable for higher fundamental frequencies.

Low suppression of higher harmonics of the source of the fundamental frequency may represent an important source of errors. In the case of the measurements presented above, signal sources with high suppression of higher harmonics were used together with high-quality filters, thus this influence can be considered as negligible.

Measurements at higher power levels and for lower harmonic suppressions may be negatively influenced by the mutual interaction of generators due to insufficient isolation and also by reflections between generators and the measured sensor. These errors may be reduced by using a more complex setup with selective levelling possibility for both the fundamental frequency signal and the higher harmonic component.

8. Conclusion

A method is described for evaluating the influence of higher harmonic components on the measurement uncertainty when measuring power using diode power sensors. It was shown for several power sensor types that the errors in the whole dynamic range of the sensors for various harmonic suppressions can be estimated with acceptable accuracy from only several measurements in the transition region above the square-law region with harmonic suppression approx. -15 dBc to -20 dBc. Practical measurement setup is shown which is also suitable for characterization of sensors from other vendors. It was also shown, by both modelling and measurements, that not all power sensors with detectors operating significantly above the square-law region show the peak detecting behaviour.

Acknowledgement

This work was supported by the project 15RPT01 RFMicrowave. This project has received funding from the EMPIR programme co-financed by the Participating States and from the European Union's Horizon 2020 research and innovation programme.

References

[1] Y. Abdo, M. Celep, "New Effective Coaxial Twin-Load Micro-calorimeter System," *Proc. of Conference on Precision Electromagnetic Measurements (CPEM)*, Ottawa, ON, 2016, pp. 1-2.

[2] Rohde & Schwarz, "Voltage and power measurements," PD 757.0835.23.

[3] Agilent, "Fundamentals of RF and microwave power measurements", NA 64-1A, 5989-6255EN, 1998.

[4] Principles of Power Measurement, Boonton, 2011 [online], available: http://boonton.com/forms/principles-of-power-measurement-form

[5] Rohde & Schwarz, "Program for Measurement Uncertainty Analysis with R & S Power Meters", AN 1GP43_0E, 2001.

[6] A. Fantom (ed.): *Radio frequency & microwave power measurement*, IEE Electrical measurement series 7, Peter Peregrinus Ltd., 1990.

[7] K. Dražil, J. Grajciar, T. Pavlíček, M. Celep, and M. Hudlička, "Harmonics Effects on Microwave Power Measurement Using Diode Sensors," *IEEE Trans. on Instrumentation and Measurement*, (accepted for publication), 2019. DOI: 10.1109/TIM.2019.2905885

[8] S. M. Sze, K. K. Ng, "*Physics of Semiconductor Devices*," 3rd ed., John Wiley & Sons, Inc., Hoboken, New Jersey, 2007.

[9] K. K. Ng, "*Complete Guide to Semiconductor Devices*," 2nd Ed., Wiley IEEE Press, Hoboken, New Jersey, 2002.

[10] M. P. Zurakowski, et al., "Diode Integrated Circuits for Millimeter-Wave Applications," *Hewlett Packard Journal*, November 1986, pp. 14-21. http://hparchive.com/Journals/HPJ-1986-11.pdf

[11] S. Wetenkamp, "Comparison of Single Diode Vs. Dual Diode Detectors for Microwave Power Detection," *Proc. of IEEE MTT-S International Microwave Symposium Digest*, Boston, MA, USA, 1983, pp. 361-363.

[12] G. Massobrio, P. Antognetti, "*Semiconductor Device Modeling with SPICE*," McGraw-Hill, 1993.

[13] Diode Detector Simulation using Agilent Technologies EEsof ADS Software, Agilent Technologies Application Note 1156, 1999.

[14] HSMS-286x Series Surface Mount Microwave Schottky Detector Diodes, Agilent Technologies [online], available: http://www.crystal-radio.eu/hsms286xdata.pdf